A study of conical intersection effects on scattering processes: The validity of adiabatic singlesurface approximations within a quasiJahn–Teller model

Roi Baer, David M. Charutz, Ronnie Kosloff, and Michael Baer

Citation: The Journal of Chemical Physics **105**, 9141 (1996); doi: 10.1063/1.472748
View online: http://dx.doi.org/10.1063/1.472748
View Table of Contents: http://scitation.aip.org/content/aip/journal/jcp/105/20?ver=pdfcov
Published by the AIP Publishing

A study of conical intersection effects on scattering processes: The validity of adiabatic single-surface approximations within a quasi-Jahn–Teller model

Roi Baer
The Fritz Haber Institute for Molecular Dynamics, The Hebrew University, Jerusalem, Israel

David M. Charutz
Department of Physics and Applied Mathematics, SOREQ NRC, Yavne 81800, Israel

Ronnie Kosloff
The Fritz Haber Institute for Molecular Dynamics, The Hebrew University, Jerusalem, Israel

Michael Baer
Department of Physics and Applied Mathematics, SOREQ NRC, Yavne 81800, Israel

(Received 4 April 1996; accepted 10 June 1996)

Conical intersections between Born–Oppenheimer potential energy surfaces create singularities which are known to have a direct effect on the symmetry of the nuclear wave functions. In this article is presented a quasi-Jahn–Teller model to study the symmetry effects of these singularities on nonreactive and reactive scattering processes. Applying this model, we were able to determine in what way and to what extent the conical intersection affects the relevant *S*-matrix elements. Having the results of this study available, conclusions concerning more realistic systems were derived. © *1996 American Institute of Physics.* [S0021-9606(96)00135-3]

I. INTRODUCTION

The conical intersection between Born–Oppenheimer potential energy surfaces (PES) is an important and a well studied subject within molecular physics. One of the most well known effects related to this subject is the Jahn–Teller (JT) effect which is a characteristic effect for systems with three identical atoms.[1–6] It turns out that at the point of the conical intersection the Born–Oppenheimer (BO) treatment[7] yields a singularity strong enough to affect symmetry properties of the system under consideration. These facts are well known but were, so far, treated mainly for bound systems.[8–10]

In the present study we extended the JT model, which was originally devised for bound systems, to a scattering process. This enabled us to see, for the first time in a relatively simple two-coordinate model, the effect of symmetry on characteristic scattering magnitudes. More specifically, we calculated inelastic and reactive *S*-matrix elements in several ways: First by doing two-surface calculations in order to see, among other things, to what extent the symmetry affects the various transition probabilities and second by doing two approximate single-surface calculations in order to see to what extent these effects can correctly be reproduced. The model, although being very simple as compared to the complicated three dimensional nonreactive and reactive triatom systems, is still realistic enough and consequently general conclusions can be drawn from it.

Nonadiabatic effects are usually important when electronic states become degenerate along a region in space configuration. In such cases the nonadiabatic coupling terms behave in a very abrupt way producing numerical instabilities that either cannot be treated or cause the final numerical results to be not reliable enough.[11] Consequently it was suggested to change the representation, namely, to move from the adiabatic to the diabatic representation where these coupling terms are eliminated altogether.[11–13] This transition is performed by an orthogonal transformation which in case of a two-surface system is characterized by an angle α—the adiabatic–diabatic angle.[11,12] One of the present authors[11] showed how α can be calculated in a general case and it turns out that usually it is a complicated function of the spatial coordinates. However, for the JT model it was shown that this angle is a very simple function of the coordinates namely it is equal to $(\varphi/2)$, where φ is the (planar) polar coordinate.[8,9]

The possible effects of conical intersections on scattering processes became recently a major issue.[14,15] It was claimed that ignoring them in (single-surface) quantum mechanical treatments may lead to erroneous results for such systems as the $H+H_2$ system and its isotopic analogs.[14] To show that this is really the case Kuppermann *et al.*[15(a)–15(c)] considered some of these systems in three dimensions not by performing two-surface calculations but carried out new single-surface calculations modified by including a phase factor to correct for the nonuniqueness (namely changing sign when encircling the point of the conical intersection) of the *electronic* basis set. By doing that the nuclear wave function was forced to change sign as well so that the total wave function (the one formed by the product of the two) is single-valued everywhere. Some of the calculated magnitudes, in particularly those related to the phases of the *S*-matrix elements, were shown to be affected significantly by the incorporation of the phase factor. This situation is reminiscent of a well known class of physical problems associated with the Aharonov–Bohm[16] effect and with a wider range of problems associated with the Berry phase.[17]

The simplest phase factor to give the right change of sign is $(\varphi/2)$ or more general $(2n+1)(\varphi/2)$ where n is an integer.[4–6,8,14,15] The question to be asked is whether such a modification is enough to correct for the effect of the conical intersection in a general case. In our present derivation we show that the ''natural'' choice for phase factor is the above mentioned adiabatic–diabatic transformation angle α. The difficulty encountered with this (general) result is that in case of the present JT model the angle α is equal to $\varphi/2$ and consequently, within this model, it is not possible to distinguish between the two angles namely to tell us which one of the two will yield the correct results as obtained in a more general two-surface system.

In the next chapter is given, first, a theoretical background for treating multisurface systems, and then the details related to the quasi-*JT scattering model*; in the third chapter are described several PESs which are used within the present quasi-JT model and for which are calculated the S-matrix elements; in the fourth chapter are presented the numerical approaches applied here to solve the various Schrodinger equations (SE); in the fifth are shown and discussed the results and in the sixth are summarized the conclusions.

II. THEORY

A. The general approach

The SE that describes the motion of the electrons and the nuclei is given in the form

$$(T_n+H_e)\Psi=E\Psi, \tag{1}$$

where T_n is the nuclear kinetic energy operator, H_e is the electronic Hamiltonian, E is the total energy, n and e stand for nuclear and electronic coordinates, respectively, and Ψ is the total nuclear-electronic wave function. In what follows Ψ will be expanded in the form[7]

$$\Psi=\sum_{i=1}^{M}\chi_i(n)\zeta_i(e;n), \tag{2}$$

where the $\zeta_i(e;n)$'s are a complete set of electronic eigenfunctions and the $\chi_i(n)$'s, the coefficients, are considered to be the nuclear wave functions related to the ith electronic state. The $\zeta_i(e;n)$'s which depend parametrically on the nuclear coordinates are solutions of the following eigenvalue problem:

$$\{H_e-u_i(n)\}\zeta_i(e;n)=0; \quad i=1,\ldots,M, \tag{3}$$

where the $u_i(n)$; $i=1,..,M$, the eigenvalues, are the adiabatic PESs.

Substituting Eq. (2) in Eq. (1) while recalling Eq. (3), multiplying it by $\zeta_j(e;n)$ and integrating over electronic coordinates yields[11,12]

$$\left\langle \zeta_j(e;n)\middle| T_n\sum_i \zeta_i(e;n)\chi_i(n)\right\rangle + \{u_j(n)-E\}\chi_j=0; \quad j=1,\ldots,M. \tag{4}$$

Since

$$T_n=-\frac{1}{2m}\nabla^2, \tag{5}$$

where

$$\nabla=\left(\frac{\partial}{\partial q_1},\frac{\partial}{\partial q_2},\ldots,\frac{\partial}{\partial q_N}\right) \tag{6}$$

we get for Eq. (4)

$$-\frac{1}{2m}\sum_j^M[(\delta_{ij}\nabla^2+2\tau_{ij}^{(1)}\nabla+\tau_{ij}^{(2)})\chi_j(q_1,q_2,\ldots)] + [u_i(q_1,q_2,\ldots)-E]\chi_i(q_1,q_2,\ldots)=0, \tag{7}$$

where

$$\tau_{ij}^{(1)}=\langle\zeta_1|\nabla\zeta_j\rangle; \quad \tau_{ij}^{(2)}=\langle\zeta_1|\nabla^2\zeta_j\rangle. \tag{8}$$

In what follows we will concentrate on the two-surface case. Thus Eq. (7) becomes

$$\left[-\frac{1}{2m}\nabla^2+\overline{u_1}-E\right]\chi_1-\frac{1}{m}\boldsymbol{\tau}^{(1)}\cdot\nabla\chi_2-\frac{1}{2m}\nabla\boldsymbol{\tau}^{(1)}\chi_2=0,$$
$$\left[-\frac{1}{2m}\nabla^2+\overline{u_1}-E\right]\chi_2+\frac{1}{m}\boldsymbol{\tau}^{(1)}\cdot\nabla\chi_1+\frac{1}{2m}\nabla\boldsymbol{\tau}^{(1)}\chi_1=0, \tag{9}$$

where $\boldsymbol{\tau}^{(1)}(=\tau_{12}^{(1)})$ is a vector who's components are scalars (not matrices) and the $\overline{u_i}$'s are given in the form

$$\overline{u_i}=u_i+\frac{1}{2m}\boldsymbol{\tau}^{(1)^2}; \quad i=1,2. \tag{10}$$

Here we made use of the fact that $\boldsymbol{\tau}^{(2)}$ is a matrix that is related to $\boldsymbol{\tau}^{(1)}$ in the following way:

$$\boldsymbol{\tau}^{(2)}=\nabla\cdot\boldsymbol{\tau}^{(1)}+(\boldsymbol{\tau}^{(1)})^2. \tag{11}$$

A SE that is diagonal in the kinetic operator yields single-valued functions as solutions. Thus as long as such equations are encountered no difficulties with respect to the uniqueness of the solutions are anticipated. However, it turns out that the Born–Oppenheimer treatment leads to a nuclear hamiltonian that contains nondiagonal kinetic operators, in particularly, the one with respect to the translational coordinate. This fact guarantees that the nuclear wave functions, when properly calculated, will be of the right symmetry to ensure an overall *electronic-nuclear* single-valued solution. It is well noticed that the parameters which govern the symmetry features of the solution are the nonadiabatic coupling terms and therefore it is important always to incorporate them, also, when approximations are employed. A situation where they are ignored is when one applies the usual BO approximation.[7] In case of Eq. (9) the ordinary BO approximation will yield the equation

$$\left(-\frac{1}{2m}\nabla^2+u-E\right)\chi=0. \tag{12}$$

Equation (12) produces singled valued solutions and therefore when a multivalued solution is required this equation may lead to erroneous results. It was shown elsewhere[18] that in case the energy is significantly below the upper surface at every point in configuration space the following equation:

$$\frac{1}{2m}[-\nabla^2+\overline{u_1}-E]\chi+\frac{i}{m}\,\tau^{(1)}\cdot\nabla\chi+\frac{i}{2m}\,\nabla\tau^{(1)}\chi=0 \tag{13}$$

is, in fact, the relevant equation. It is seen that Eqs. (12) and (13) are very similar except for two additional terms in Eq. (13) which are missing in Eq. (12). These additional terms as will be shown later, enable to incorporate the proper boundary conditions so that the solution will have the right symmetry. Equation (13) can be considered as an extended version of the BO approximation.

In the next chapter are presented solutions for Eqs. (9), (12), and (13) for three different types of scattering problems.

B. The quasi-Jahn–Teller model

In this article we will study a two-coordinate quasi-''JT scattering'' model in which the harmonic oscillator potential q^2 and the linear (potential) coupling term q are replaced by two more general potentials $F(q,\varphi)$ and $G(q,\varphi)$, respectively. Here, like in the original JT model, q is a radial coordinate, and φ the corresponding polar coordinate.

Following Longuet-Higgins *et al.*,[4] a model Hamiltonian that describes the atomic system within a degenerate manifold of electronic states ζ_i, $i=1,\ldots,N$ coupled to a nuclear system is given in the form

$$H=-\tfrac{1}{2}E_{\rm el}\frac{\partial^2}{\partial\theta^2}+T_n+F(q,\varphi)-G(q,\varphi)\cos(2\theta-\varphi), \tag{14}$$

where $E_{\rm el}$ is a characteristic electronic energy value, θ is an electronic phase angle, q and φ are, as mentioned earlier, nuclear coordinates and T_n is the nuclear kinetic operator described in terms of polar coordinates

$$T_n=-\frac{1}{2m}\left[\frac{\partial^2}{\partial q^2}+\frac{1}{q}\frac{\partial}{\partial q}+\frac{1}{q^2}\frac{\partial^2}{\partial\varphi^2}\right]. \tag{15}$$

Following the theory presented earlier [see Eq. (2)] the electronic eigenfunctions are solutions of the following electronic SE:

$$\left(-\frac{1}{2}\,E_{\rm el}\frac{\partial^2}{\partial\theta^2}-G(q,\varphi)\cos(2\theta-\varphi)-\widetilde{u}_i(q,\varphi)\right)\zeta_i(\theta,q,\varphi)=0, \tag{16}$$

where $\widetilde{u}_i(q,\varphi)$ are the electronic eigenvalues.

In Appendix A is shown that the *approximate* solutions of Eq. (16), related to the two lowest eigenvalues, are

$$\zeta_1=\frac{1}{\sqrt{\pi}}\cos(\theta-\tfrac{1}{2}\varphi)\quad\text{and}\quad\zeta_2=\frac{1}{\sqrt{\pi}}\sin(\theta-\tfrac{1}{2}\varphi). \tag{17}$$

It is noticed that the two electronic functions are not single-valued with respect to φ (a nuclear coordinate). Thus if we want the total wave function to be single-valued with respect to φ we have to form nuclear wave functions that have the same symmetry as the electronic wave functions.

The eigenvalues of Eq. (16) are

$$\widetilde{u}_i=\tfrac{1}{2}E_{\rm el}\mp G(q,\varphi);\quad i=1,2 \tag{18}$$

and therefore, recalling Eq. (14), the two lowest adiabatic PESs are

$$u_i(q,\varphi)=F(q,\varphi)+\widetilde{u}_i(q,\varphi);\quad i=1,2 \tag{19}$$

Following the derivations of the previous Section, we are now in position to present the two adiabatic coupled equations to be solved [see Eq. (9)]

$$\begin{aligned}&[T_n+\overline{u_1}-E]\chi_1+\frac{1}{2mq^2}\frac{\partial}{\partial\varphi}\chi_2=0,\\&[T_n+\overline{u_2}-E]\chi_2-\frac{1}{2mq^2}\frac{\partial}{\partial\varphi}\chi_1=0,\end{aligned} \tag{20}$$

where

$$\overline{u_i}=u_i+\frac{1}{8mq^2};\quad i=1,2. \tag{21}$$

Equations (20) can be solved as such but we prefer to do it by transforming to the diabatic representation. This is done employing the following adiabatic–diabatic transformation (details about this transformation can be found in Ref. 11):

$$\begin{pmatrix}\chi_1\\ \chi_2\end{pmatrix}=\begin{pmatrix}\cos\alpha & -\sin\alpha\\ \sin\alpha & \cos\alpha\end{pmatrix}\begin{pmatrix}\eta_1\\ \eta_2\end{pmatrix}. \tag{22}$$

Substituting Eq. (22) in Eq. (20) it can be shown[9,11] that choosing α to be

$$\alpha=\tfrac{1}{2}\varphi \tag{23}$$

annihilates the coefficients of the first derivatives and leads to the following (diabatic) equations:

$$\begin{aligned}&\{T_n+\tfrac{1}{2}E_{\rm el}+F(q,\varphi)-G(q,\varphi)\cos\varphi\}\eta_1\\&\quad-G(q,\varphi)\sin\varphi\,\eta_2=E\,\eta_1,\\&\{T_n+\tfrac{1}{2}E_{\rm el}+F(q,\varphi)+G(q,\varphi)\cos\varphi\}\eta_2\\&\quad-G(q,\varphi)\sin\varphi\,\eta_1=E\,\eta_2.\end{aligned} \tag{24}$$

Equation (24) is a set of equations which does not contain the first derivative terms and therefore will produce a single-valued solution. However, the two relevant (adiabatic) solutions (χ_1,χ_2) given in Eq. (22) with α being equal to $(\varphi/2)$ are of the right symmetry and therefore yield an overall single-valued wave function Ψ [see Eq. (1)].

C. Approximate single-surface equations

In what follows we discuss two approaches to obtain a relevant single surface equation:

(a) The conventional approach is to employ the BO approximation which means simply ignoring the coupling between the various PESs. Thus the equation for χ_1 (in what follows the index 1 will be omitted unless we consider a two-surface case) is

$$(T_n+u-E)\chi=0. \tag{25}$$

As was already mentioned earlier this equation does not yield a solution with the proper symmetry (namely, the prod-

uct $\chi\zeta$ is not single-valued with respect to φ) and consequently may lead, in cases the symmetry affects the calculations, to erroneous results.

(b) The other approximate solution will be obtained by considering Eq. (13)

$$\left(T_n+\overline{u}-\frac{i}{2mq^2}\frac{\partial}{\partial\varphi}-E\right)\widetilde{\chi}=0, \tag{13'}$$

where

$$\overline{u}=u+\frac{1}{8mq^2}. \tag{21'}$$

Equation (13′), as will be shown in the following sections, yields a solution with the relevant symmetry and consequently to the correct transition probabilities.

III. THE JAHN–TELLER "SCATTERING" MODEL

Our starting point are two adiabatic PESs u_i; $i=1,2$ which appear in Eqs. (3) and (7). The lower PES $u_1(R,r)$ is given in the form

$$u_1(R,r)=\tfrac{1}{2}m(\omega_0-\widetilde{\omega}_1(R))^2r^2+Af(R,r)+g(R) \tag{26a}$$

and the upper one in the form

$$u_2(R,r)=\tfrac{1}{2}m\omega_0^2r^2-(D-A)f(R,r)+D. \tag{26b}$$

Here, R and r are the Cartesian coordinates (defined in the intervals: $-\infty\leqslant R\leqslant\infty$ and $-\infty\leqslant r\leqslant\infty$) related to q and φ in the following way:

$$r=q\ \sin\ \varphi \quad \text{and} \quad R=q\ \cos\ \varphi. \tag{27}$$

In our model R is the reaction (translational) coordinate and r the (vibrational) internal coordinate. The function $\varpi_1(R)$ is an R dependent function of the form

$$\widetilde{\omega}_1(R)=\omega_1\ \exp(-(R/\sigma_1)^2) \tag{28}$$

The two functions $f(R,r)$ and $g(R)$ are chosen in such a way to form the three required models we intend to study.

A. The reactive double slit model (RDSM)

In this case $g(R)\equiv 0$ along the whole R interval and $f(R,r)$ is chosen to be a Gaussian which peaks at (0,0), namely,

$$f(R,r)=\exp\left(-\frac{R^2+r^2}{\sigma^2}\right). \tag{29}$$

It is well noticed that with this choice the two adiabatic PESs are well separated from each other and touch only at one point namely at the origin. In Fig. 1 are shown the two surfaces forming the double slit on the lower surface. It is well noticed that the range of R is $[-\infty,\infty]$ where $R=\infty$ is the reagents asymptote and $R=-\infty$ is the products asymptote. The transition state is located around $R=0$. The lower adiabatic bound potential curve (along r) at $R=0$, as well as the corresponding eigenvalues, are shown in Fig. 2.

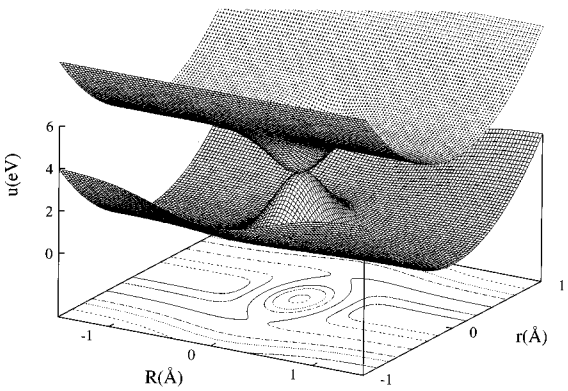

FIG. 1. The two adiabatic potential energy surfaces applied in the quasi-Jahn–Teller model.

B. The reactive single slit model (RSSM)

In this case, again, $g(R)\equiv 0$ but $f(R,r)$ is chosen to be a product of two functions

$$f(R,r)=a(R)b(r), \tag{30}$$

where $a(R)$ is a Gaussian, namely,

$$a(R)=\exp(-(R/\sigma)^2), \tag{31}$$

and $b(r)$ is an Eckart-type potential[19]

$$b(r)=\frac{cy}{(1+y)}+\frac{dy}{(1+y)^2}. \tag{32}$$

Here, $y=\exp(-(r/l))$ and c, d, and l are constants. As in the previous case the PESs are well separated but touch at one point which is now removed from the origin. The potential curve along r at $R=0$ and the corresponding eigenvalues are shown in Fig. 3.

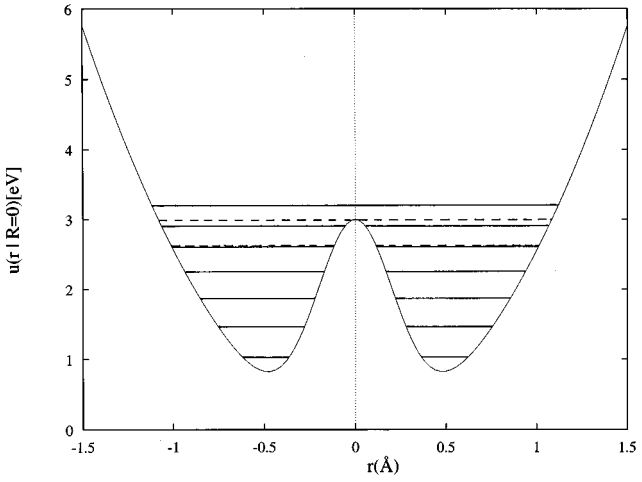

FIG. 2. A cross-section of the lower adiabatic potential along the vibrational coordinate r at $R=0$ as calculated for the reactive-double-slit-model (RDSM). The horizontal lines stand for the corresponding vibrational eigenstates.

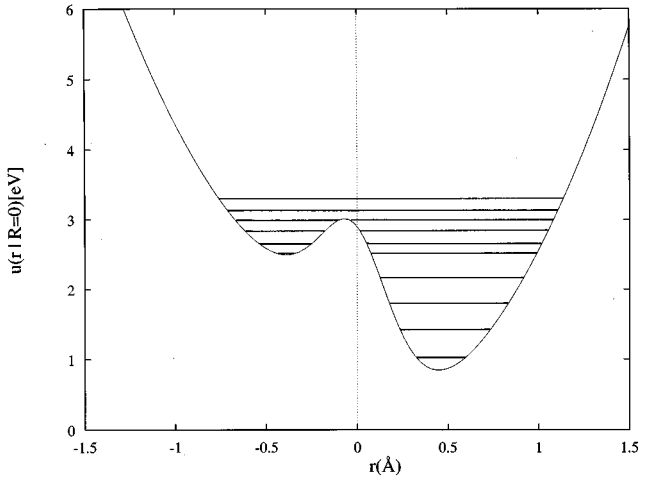

FIG. 3. A cross-section of the lower adiabatic potential along the vibrational coordinate r at $R=0$ as calculated for the reactive-single-slit-model (RSSM). The horizontal lines stand for the corresponding vibrational eigenstates.

C. The nonreactive double slit model (NDSM)

The PESs in this case are identical to one defined in case (a) except that $g(R)$ is now different from zero. It will be assumed to be of the form

$$g(R)=\exp(-[R-R_f)/\rho], \tag{33}$$

where R_f is negative with an absolute value large enough so that the nonzero interval of this potential is far enough from the origin (the coefficient in front of the exponential is 1.0 eV). The addition of $g(R)$ converts the original reactive potential to a nonreactive potential as can be seen from Fig. 4 where is presented the potential along the reaction coordinate R, namely, $u_1(R,r=0)$.

All numerical values attached to the various constants are presented in Table I.

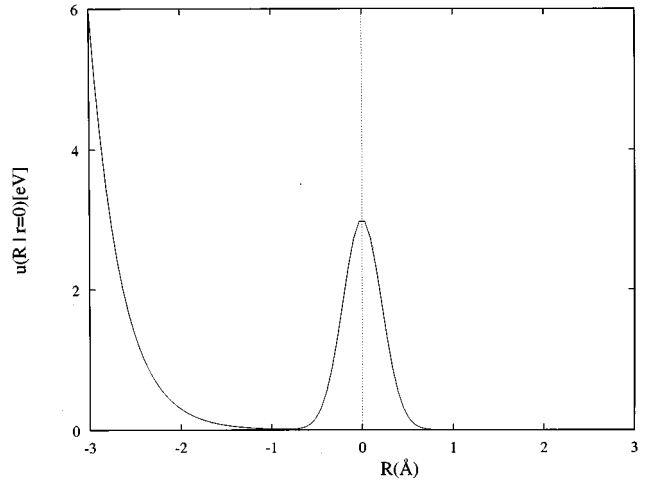

FIG. 4. The potential of the lower adiabatic potential along the reaction coordinate R at $r=0$ as calculated for the nonreactive-double-slit-model (NDSM).

TABLE I. List of parameters applied in the calculations.

All models	
m	0.58 Proton Mass
A	3.0 eV
D	5.0 eV
σ	0.30 Å
σ_1	0.75 Å
ω_0	39.14×10^{13} s^{-1}
ω_1	7.83×10^{13} s^{-1}
RSSM only	
c	1.8 eV
d	8.0 eV
l	0.135 Å
NDSM only	
ρ	0.333 Å
R_f	−2.403 Å

As was described earlier the two-surface case will be treated in the diabatic representation. Consequently having determined u_1 and u_2 we are now in position to present the diabatic potential matrix.[9,11] Thus,

$$\begin{aligned} W_{11}&=\tfrac{1}{2}[u_1+u_2+(u_1-u_2)\cos\varphi],\\ W_{22}&=\tfrac{1}{2}[u_1+u_2-(u_1-u_2)\cos\varphi],\\ W_{12}&=\tfrac{1}{2}(u_1-u_2)\sin\varphi, \end{aligned} \tag{34}$$

where φ was defined in terms of Eqs. (27). The two diabatic PESs are shown in Fig. 5.

IV. THE NUMERICAL TREATMENT

In what follows are described two methods to solve the various differential equations presented in Sec. II. We used both in order to guarantee that the final results are correct and well converged.

A. The discrete-variable-representation (DVR)-Toeplitz method

Most of the calculations were carried out employing this method. In what follows is described how each case is treated within this approach.

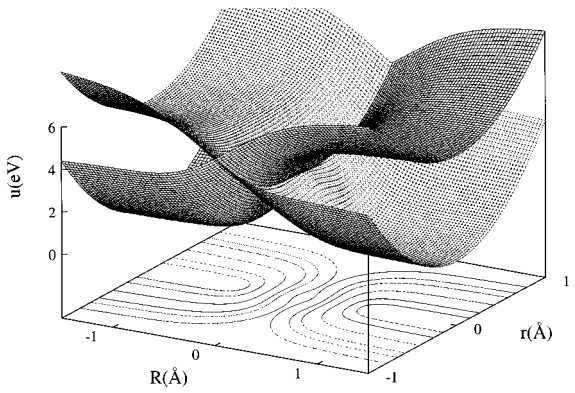

FIG. 5. The two diabatic potential energy surfaces applied in the extended Jahn–Teller model for the reactive-double-slit-model (RDSM).

1. The treatment of the two-surface case

Our derivation applies to Eq. (24) [see also Eq. (34)] and it will be solved by applying the perturbative approach, namely (η_1,η_2) will be replaced by (ξ_1,ξ_2) where the two are related in the following way:

$$\eta_1=\xi_1+\phi_{10},$$
$$\eta_2=\xi_2. \tag{35}$$

Here, ϕ_{10} is a solution of an unperturbed single surface equation of the kind

$$[T_n+U(R,r)-E]\phi_{10}=0 \tag{36}$$

where T_n is of the form

$$T_n=-\frac{1}{2m}\left[\frac{\partial^2}{\partial R^2}+\frac{\partial^2}{\partial r^2}\right] \tag{37}$$

and $U(R,r)$ is a separable potential of the form

$$U(R,r)=w(R)+v(r). \tag{38}$$

Here, $w(R)$ is an exponential decaying function of R and $v(r)$ stands for the asymptotic bound (harmonic) potential. Once ϕ_{10} is known the two coupled equations for (ξ_1,ξ_2) are[20]

$$(T_n+W_{11}-E)\xi_1+W_{12}\xi_2=V\phi_{10},$$
$$(T_n+W_{22}-E)\xi_2+W_{12}\xi_1=W_{12}\phi_{10}, \tag{39}$$

where

$$V=W_{11}(R,r)-U(R,r). \tag{40}$$

Equations (39) are solved employing, in a most straightforward way, the DVR-Toeplitz method as was described in Ref. 21.

2. The treatment of the single surface case

In general the present case is treated in a similar way as the previous one and in this sense there is nothing to be added. However, Eq. (13′) [or Eq. (13)] behaves asymptotically as an equation with an imaginary Coulomb potential. The reason being that the first derivative term (the third term in the equation) when expressed in terms of Cartesian coordinates is of the form

$$i\,\frac{1}{q^2}\,\frac{\partial}{\partial\varphi}=i\,\frac{1}{R^2+r^2}\left(-R\,\frac{\partial}{\partial r}+r\,\frac{\partial}{\partial R}\right). \tag{41}$$

It turns out that employing the perturbativelike approach overcomes this unpleasant situation in a most straightforward way. For this, we consider the following unperturbed equation:

$$\left(T_n+\overline{U}(R,r)-i\,\frac{1}{2m(R^2+r^2)}\,\frac{\partial}{\partial\varphi}-E\right)\phi_0=0, \tag{42}$$

where

$$\overline{U}(R,r)=U(R,r)+\frac{1}{8m(R^2+r^2)} \tag{43}$$

and $U(R,r)$ is given in Eq. (38). To solve Eq. (42) we make the following substitution:

$$\phi_0(R,r)=\tilde{\phi}_0(R,r)\exp[-i(\varphi/2)] \tag{44}$$

and it is easy to show that $\tilde{\phi}_0(R,r)$ is the solution of Eq. (36). We will explicitly consider Eq. (13′) and like the two-surface case $\tilde{\chi}(R,r)$ will be written as

$$\tilde{\chi}=\xi+\phi_0, \tag{45}$$

where the equation for ξ is

$$\left(T_n+\overline{u(R,r)}-i\,\frac{1}{2m(R^2+r^2)}\,\frac{\partial}{\partial\varphi}-E\right)\xi=V\phi_0. \tag{46}$$

Here, $V(R,r)$ is defined in Eq. (40) and $\phi_0(R,r)$ is the solution of Eq. (42).

B. The Green-function Chebychev-polynomial expansion method

The scattering calculations were also performed using a new method described in Appendix B based on Chebychev-polynomial expansion of the Green function.[24–26] Here, we discuss the application of that method to the scattering Jahn–Teller problem we are addressing.

1. The two-surface diabatic case

Implementing the method described in Appendix B for the two-surface diabatic case is straightforward using the matrix Hamiltonian

$$H=T\mathbf{I}+W_{\rm di};\quad W_{\rm di}=\begin{pmatrix}W_{11} & W_{12}\\ W_{21} & W_{22}\end{pmatrix}, \tag{47}$$

where the W's are given in Eq. (34), T is the kinetic energy operator, and $\mathbf{I}$ is the 2×2 unit matrix. We assume the incoming wave to be on the lower adiabatic surface, so that we start with an adiabatic incoming $\chi^{\rm in}(\frac{1}{0})$. On this state we operate with the diabatic–adiabatic orthogonal transformation Eq. (22) to obtain the incoming diabatic state

$$\eta^{\rm in}=\begin{pmatrix}\cos\alpha\\ \sin\alpha\end{pmatrix}\chi^{\rm in}. \tag{48}$$

Note, that for a wave coming in from the negative infinity, $\alpha\to0$, so asymptotically, the diabatization matrix is actually the unit matrix. However, for a finite numerical calculation, one must use Eq. (48) as the initial state. This is essential in order to obtain good convergence.

The diabatic scattering state η is now calculated as explained in Appendix B. To obtain the transition probabilities to an outgoing adiabatic state $\chi^{\rm out}(\frac{1}{0})$, we must again first convert it to a diabatic outgoing wave

$$\eta^{\rm out}=\begin{pmatrix}\cos\alpha\\ \sin\alpha\end{pmatrix}\chi^{\rm out}, \tag{49}$$

and only then multiply it by η and integrate over r for a certain large and constant R. Since in the asymptotic outgoing channel (for $R\to\infty$) $\alpha\to\pi/2$ the diabatic outgoing state is asymptotically placed only on the second diabatic surface. However, for a finite grid calculation, it is again essential to use Eq. (49) in order to obtain convergence.

2. The single-surface case

For this case, the Hamiltonian is taken as dictated by Eqs. (13′) and (41). The boundary conditions are similar to that of a usual single-surface case, except that the incoming wave (localized by the vibrations) should be multiplied by $e^{i(\phi+\pi)/2}$ where $\phi=2\alpha$ is the polar angle. This procedure stabilizes a finite numerical calculation, since it gets rid of the global potential [Eq. (41)], which decays very slowly in the incoming channel. The same type of treatment should be applied to the outgoing states. Note, that in this case there is an important point, applying to the flux calculations if one intends to use the flux as in Eq. (B9). One should use gauge-invariant flux and add $\frac{1}{2}\nabla\phi$ to the momentum operator $-i\hbar\nabla$.

V. RESULTS AND DISCUSSION

Before starting the production we performed a series of test runs to make sure that all numerical parameters are well tuned to give correct and reliable results. In particularly we made sure that the grid steps were chosen suitable for the whole studied energy range. It is important to emphasize that this very careful selection of parameters lead, in case of the two-surface calculations, to DVR-Toeplitz (complex) matrices of size 6000×6000. The solutions of these final algebraic equations were done by the LU decoupling method.

Since one of the aims of the present calculation was to see to what extent single-surface calculations can reproduce the two-surface results and since we consider not only state-selected probabilities but also state-to-state transition probabilities we had to make sure that our results are as accurate as possible. Consequently we can guarantee in this study an accuracy of 1.0%.

Next are presented results for each of the studied PESs. Usually are shown three types of results: the exact results namely the two-surface results and the ones due to the extended BO treatment which contains the phase factor (labeled as BOPA). Results that are not always shown (because sometimes they are not relevant) are the ones due to the ordinary BO approximation (labeled BOA).

A. The reactive double-slit model (RDSM)

In this chapter are presented reactive *state-selected* probabilities and reactive and nonreactive *state-to-state* transition probabilities.

Reactive state-selected energy dependent probabilities for the four lowest initial vibrational states are presented in Fig. 6. It is important to mention that although the two surfaces are 5.0 eV apart the intersection point is at 3.0 eV. In general the fit between the three types of the results is good, also for high energies close to the intersection point. It is important to emphasize that results due to the two approximate approaches follow correctly the exact probability curve even at energies where abrupt changes take place (eventually resonances). For instance a situation like that is encountered around $E=1.7$ eV where the probability jumps from 25% to 60%. Some ''noise'' is seen to exist at the high energy interval. There the BOA results are seen to be less accurate than the BOPA results.

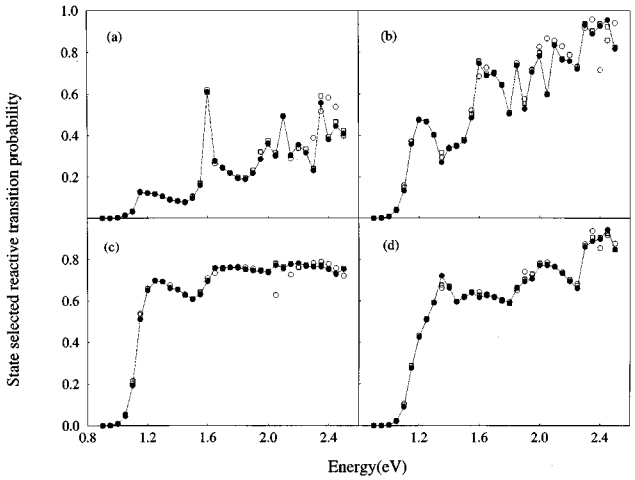

FIG. 6. State selected reactive probabilities as a function of (total) energy as calculated for the reactive-double-slit-model (RDSM). (a) Results for the ground vibrational state. (b) Results for the first excited vibrational state. (c) Results for the second excited vibrational state. (d) Results for the third excited vibrational state. —■— Results due to the two-coupled-surface calculation (exact results). ○ Results due to single-surface calculation employing the ordinary Born–Oppenheimer approximation. □ Results due to single-surface calculation employing the extended (symmetry-conserving) Born–Oppenheimer approximation.

Next are discussed the state-to-state results. At this stage it is important to emphasize that the PES assumed in this study is *even* in the vibrational coordinate (see the previous section) and therefore straightforward calculations will result in nonzero transition probabilities only between states of the same parity. Thus, one expects that $P(\text{even}\rightarrow\text{even})$ and $P(\text{odd}\rightarrow\text{odd})$ will differ from zero but $P(\text{even}\rightarrow\text{odd})$ and $P(\text{odd}\rightarrow\text{even})$ will be equal to zero. This should apply for both, the reactive and the nonreactive, transitions.

In Table II are presented various *nonreactive* state-to-state transition probabilities for four selected energies. The first row stands for the exact results and it is seen that only (even→even) and (odd→odd) probabilities are presented because these are the only ones to differ from zero. As for the approximate calculations; in most cases BOA and BOPA yield results reasonably close to the exact ones. However, there are also sometimes unexpected differences. The BOA fails almost entirely for the highest energy (i.e., $E=2.5$ eV) and sporadic differences, although not too large, can be seen at other energies for both approximations. Overall the BOPA is significantly better in simulating the exact two-surface results.

In Table III are presented various *reactive* state-to-state transition probabilities for the same four selected energies. Again the first row stands for the exact results but now only (odd→even) and (even→odd) probabilities are shown. It turns out that in contrast to the previous case the two-surface calculation results in transitions between states of different parity whereas transitions between states of the same parity, for all practical purposes, were annihilated. The calculations were repeated within the BOA and the BOPA. We show only

TABLE II. Inelastic state-to-state transition probabilities for the reactive double slit model.

E	0→0	0→2	0→4	1→1	1→3	1→5	2→2	2→4	3→3	3→5	4→4
1.0	0.292[a]	0.705	⋯	0.225	0.767	⋯	0.286	⋯	0.229	⋯	⋯
	0.289[b]	0.708	⋯	0.210	0.781	⋯	0.282	⋯	0.216	⋯	⋯
	0.289[c]	0.708	⋯	0.210	0.781	⋯	0.282	⋯	0.216	⋯	⋯
1.5	0.113	0.367	0.423	0.120	0.006	0.500	0.014	0.011	0.066	0.311	0.132
	0.114	0.363	0.419	0.115	0.004	0.498	0.017	0.011	0.062	0.312	0.127
	0.115	0.365	0.414	0.116	0.004	0.502	0.016	0.010	0.063	0.314	0.123
2.0	0.308	0.150	0.119	0.044	0.016	0.027	0.065	0.030	0.020	0.052	0.028
	0.298	0.153	0.117	0.044	0.016	0.023	0.061	0.030	0.021	0.049	0.026
	0.268	0.173	0.135	0.032	0.018	0.021	0.054	0.027	0.022	0.047	0.026
2.5	0.320	0.151	0.084	0.106	0.051	0.010	0.059	0.026	0.035	0.020	0.006
	0.310	0.149	0.081	0.104	0.050	0.011	0.058	0.027	0.036	0.020	0.008
	0.283	0.179	0.098	0.003	0.008	0.013	0.051	0.034	0.015	0.024	0.038

[a]Two-surface calculation.
[b]Single-surface calculation with phase factor.
[c]Single-surface calculation (ordinary BO approximation).

those due to the BOPA because this approximation was able to yield similar transitions as encountered in the two-surface whereas the BOA yielded transitions between states of the same parity and therefore cannot be compared with the exact results. It is noticed that the BOPA not only yields the relevant transitions but is also, quantitatively, quite reliable.

B. The nonreactive double-slit model (NDSM)

The reason for studying this model is closely related to the findings of the RDSM. Essentially what we saw was that interference phenomena formed by waves moving through the two slits managed to affect dramatically the reactive process. On the other hand, these phenomena do not seem to affect the nonreactive process. Thus we constructed a nonreactive model so that the reflected waves are forced to move back, through the two slits, to the reagents asymptotic region. The state-to-state transition probabilities for this case and for the same four energies are presented in Table IV. Again we show only nonzero transition probabilities and those are the ones between states with the same parity. Thus the interference effects did not affect the parity of the transitions.

In addition to the exact results are also presented those due to the two approximations. It is seen that the BOPA manages only partly to simulate the exact results but the BOA fails to do so in most cases. In fact the BOA produces only the lowest energy results and this can be explained by the fact that at this energy more than 90% of the incoming flux is reflected back into the reagents asymptotic region without passing the barrier at $R\sim 0$. Thus more than 90% of this reflected flux is not affected by the interference process which takes place on the reactive side only. As the energy gets higher more and more of the incoming flux passes the $R\sim 0$ region and therefore is exposed to the strong interference effects. These marks left on the reflected flux cannot be recovered by the simple BOA. The BOPA is more successful in this respect but sometimes even here non-negligible discrepancies are observed, in particular, at the higher energies.

C. The reactive single-slit model (RSSM)

In Sec. V A we established the fact that interference phenomena between waves passing through two slits, caused by the symmetry, affects dramatically the state-to-state transition probabilities and so we were curious to find out what

TABLE III. Reactive state-to-state transition probabilities for the reactive double slit model.

E	0→1	0→3	0→5	2→1	2→3	2→5	4→1	4→3	4→5
1.0	0.002[a]	0.000	⋯	0.006	0.003	⋯	⋯	⋯	⋯
	0.002[b]	0.001	⋯	0.007	0.003	⋯	⋯	⋯	⋯
1.5	0.072	0.015	0.009	0.260	0.311	0.036	0.043	0.290	0.102
	0.075	0.016	0.012	0.256	0.310	0.038	0.049	0.287	0.103
2.0	0.083	0.035	0.053	0.107	0.056	0.403	0.029	0.592	0.123
	0.082	0.042	0.058	0.103	0.054	0.409	0.021	0.596	0.114
2.5	0.003	0.019	0.142	0.033	0.105	0.231	0.011	0.467	0.092
	0.004	0.020	0.139	0.027	0.112	0.224	0.017	0.459	0.090

[a]Two-surface calculation.
[b]Single-surface calculation with phase factor.

TABLE IV. Inelastic state-to-state transition probabilities for the non-reactive double slit model.

E	0→0	0→2	0→4	1→1	1→3	1→5	2→2	2→4	3→3	3→5	4→4
1.0	0.290[a]	0.709	⋯	0.229	0.771	⋯	0.290	⋯	0.229	⋯	⋯
	0.286[b]	0.714	⋯	0.215	0.785	⋯	0.286	⋯	0.215	⋯	⋯
	0.287[c]	0.713	⋯	0.213	0.787	⋯	0.287	⋯	0.213	⋯	⋯
1.5	0.088	0.537	0.374	0.165	0.253	0.581	0.304	0.158	0.349	0.397	0.467
	0.089	0.549	0.362	0.225	0.249	0.526	0.302	0.149	0.288	0.463	0.489
	0.232	0.174	0.593	0.362	0.177	0.461	0.732	0.094	0.308	0.514	0.313
2.0	0.030	0.541	0.205	0.314	0.387	0.142	0.144	0.069	0.100	0.078	0.643
	0.029	0.549	0.206	0.262	0.483	0.100	0.135	0.074	0.080	0.060	0.622
	0.185	0.511	0.248	0.421	0.154	0.067	0.288	0.058	0.108	0.469	0.506
2.5	0.032	0.574	0.231	0.244	0.175	0.210	0.137	0.029	0.591	0.143	0.522
	0.029	0.551	0.246	0.216	0.213	0.231	0.167	0.034	0.644	0.102	0.501
	0.101	0.201	0.328	0.536	0.168	0.007	0.564	0.178	0.206	0.119	0.076

[a]Two-surface calculation.
[b]Single-surface calculation with phase factor.
[c]Single-surface calculation (ordinary BO approximation).

kind of an effect will have the symmetry on a single-slit model. In Table V are presented state-to-state reactive and nonreactive probabilities as calculated for $E=2.0$ eV. It is noticed that overall the exact results and the ones due to the two models are very similar, a fact which means that at least in such a case the symmetry has, at most, a negligible effect on the probabilities.

VI. CONCLUSIONS

In this article is treated a generalized JT model which enabled the study of symmetry effects on scattering processes. More specifically we examined a two-coordinate JT ''reactive'' type model which allows interference phenomena while the system is moving from the reagents to the products regions.

We started the article with presenting a general theoretical background which not only results in the relevant SE to describe the motion of the system on several (two) coupled PESs but also showed the way to two approximate single-surface SEs: The one is the ordinary BO approximation which usually yields relevant results as long as the second PES is far enough but fails to treat symmetry effects (in case they are important). The other is an extended BO approximation [see Eq. (13)], introduced here to our knowledge for the first time, in which phase-factor effects are included and therefore is expected to be able to treat correctly also symmetry phenomena.

To carry out the numerical study we considered three different types of PESs: two reactive and one nonreactive. The reactive ones were chosen in such a way that one of them exposes symmetry effects and the other does not whereas the non reactive may or may not expose symmetry effects depending on the kinetic energy.

In the numerical study we derived first, the two-surface results which are considered to be the exact ones and then tried to reproduce them by applying the two types of BO approximations. It turned out that the BOPA simulates correctly almost all two-surface transition probabilities whether being state-selected or state-to-state ones. The ordinary BO approximation simulated correctly the state-selected probabilities and in one case (i.e., for RSSM where symmetry effects are not expected) also the state-to-state transition probabilities.

Symmetry effects are expected for systems with conical intersections. However, in order for them to be noticed some very unusual situations have to exist. We have shown that this can happen with a wave (packet) that is forced to pass through two slits and then combines again to form a single wave (packet). However, this is a very rare situation. In case of a real reactive system the two slits usually lead to two different arrangements and so the bifurcated wave packets have a low probability to interfere with each other while receding from the interaction region. In our opinion, if at all there is possibility for these effects to be seen, they should be looked after in nonreactive processes. In a nonreactive process the eventually bifurcated wave packet unites again to return through the same arrangement after surrounding (or encircling) the conical intersection point.

ACKNOWLEDGMENTS

One of the authors (M.B.) would like to thank R. Englman for many illuminating discussions regarding Jahn–Teller model and related subjects. As well he appreciates comments from D. Yarkoni, L. S. Cederbaum, B. Keudriek, and R. T Pack.

APPENDIX A: THE TWO LOWEST EIGENVALUES AND THE CORRESPONDING ELECTRONIC EIGENFUNCTIONS FOR THE GENERALIZED JAHN–TELLER MODEL

In this appendix we derive two approximate solutions of the eigenequation Eq. (16). For this sake ζ (in what follows the subscripts will be ignored) will be expanded in the following form:

TABLE V. State-to-state transition probabilities for the reactive single slit model for $E=2.0$ eV.

v_f	$v_i=$ 0	1	2	3	4	5	6	7	Total
Reactive									
0	0.014[a]	0.008	0.010	0.031	0.004	0.031	0.096	0.070	0.264
	0.016[b]	0.008	0.009	0.034	0.005	0.039	0.100	0.062	0.272
	0.016[c]	0.008	0.010	0.033	0.005	0.032	0.099	0.068	0.271
1		0.008	0.029	0.042	0.013	0.086	0.168	0.105	0.459
		0.007	0.027	0.047	0.015	0.106	0.168	0.088	0.465
		0.005	0.033	0.045	0.015	0.088	0.170	0.099	0.462
2			0.041	0.043	0.070	0.087	0.063	0.023	0.366
			0.040	0.039	0.078	0.097	0.057	0.017	0.369
			0.040	0.047	0.069	0.088	0.061	0.020	0.369
3				0.119	0.123	0.043	0.010	0.011	0.422
				0.104	0.134	0.038	0.014	0.012	0.423
				0.113	0.120	0.042	0.012	0.012	0.424
Nonreactive									
0	0.389	0.059	0.028	0.075	0.020	0.063	0.020	0.082	0.735
	0.381	0.062	0.026	0.075	0.022	0.061	0.021	0.083	0.730
	0.381	0.062	0.026	0.074	0.022	0.061	0.021	0.083	0.729
1		0.207	0.112	0.108	0.039	0.000	0.003	0.012	0.540
		0.203	0.114	0.106	0.039	0.000	0.003	0.012	0.538
		0.204	0.113	0.107	0.039	0.000	0.003	0.011	0.538
2			0.243	0.033	0.060	0.091	0.001	0.064	0.634
			0.246	0.034	0.054	0.091	0.002	0.065	0.631
			0.246	0.034	0.055	0.091	0.002	0.065	0.631
3				0.176	0.092	0.056	0.021	0.017	0.578
				0.176	0.091	0.056	0.021	0.016	0.576
				0.176	0.090	0.056	0.021	0.016	0.576

[a]Two-surface calculation.
[b]Single-surface calculation with phase factor.
[c]Single-surface calculation (ordinary BO approximation).

$$\zeta=\sum_n a_n \cos^n\left(\theta-\frac{\varphi}{2}\right). \tag{A1}$$

Substituting Eq. (A1) in Eq. (16) where we also apply the following trigonometric relation:

$$\cos(2\theta-\varphi)=2\cos^2\left(\theta-\frac{\varphi}{2}\right)-1 \tag{A2}$$

leads to the following equation:

$$-\frac{1}{2}E_{\rm el}\sum_{n=0}[a_{n+2}(n+2)(n+1)-a_n n^2]\cos^n\left(\theta-\frac{\varphi}{2}\right)$$
$$-2G\sum_{n=0}a_n\cos^{n+2}\left(\theta-\frac{\varphi}{2}\right)$$
$$+(G-u)\sum_{n=0}a_n\cos^n\left(\theta-\frac{\varphi}{2}\right)=0 \tag{A3}$$

From Eq. (A3) we get the general equation for the coefficients a_n, namely:

$$-\tfrac{1}{2}E_{\rm el}(n+2)(n+1)a_{n+2}+(\tfrac{1}{2}E_{\rm el}n^2+(G-u))a_n-2Ga_{n-2}=0. \tag{A4}$$

Since all subscripts have to be positive the initial value of n can be either $n=0$ [for the even powers in Eq. (A1)] or $n=1$ (for the odd powers). A simple approximate solution is obtained for the odd series. Here, assuming $n=1$, ignoring the third term, we get that $a_1\neq 0$ and by choosing $u(q,\varphi)$, the lowest eigenvalue, to be

$$u(q,\varphi)=\tfrac{1}{2}E_{\rm el}+G(q,\varphi) \tag{A5}$$

we get that $a_3=0$ and consequently ζ is, approximately, given in the form

$$\zeta(\theta,\varphi)=\Gamma\cos\left(\theta-\frac{\varphi}{2}\right), \tag{A6}$$

where Γ is a constant.

The second (independent) solution of Eq. (16) is obtained by assuming ζ to be of the form

$$\zeta=\sum_n a_n \sin^n\left(\theta-\frac{\varphi}{2}\right), \tag{A7}$$

and in a similar way as before one can show that for this type of solution the lowest electronic eigenvalue is of the form

$$u(q,\varphi)=\tfrac{1}{2}E_{\rm el}-G(q,\varphi), \tag{A8}$$

and the corresponding approximate eigenfunction is

$$\zeta(\theta,\varphi)=\Gamma\ \sin\left(\theta-\frac{\varphi}{2}\right). \tag{A9}$$

This completes the derivations.

APPENDIX B: GENERAL METHOD FOR SCATTERING CALCULATIONS: THE GREEN'S FUNCTION EXPANSION IN A CHEBYSCHEV SERIES

In this appendix we describe to some detail the second method we have employed in the calculations showed in this paper. This scheme is based on expanding the Green's function as a Chebychev series. We describe here the general approach, while the applications to the single-surface and the two-surface cases are discussed in the main body of the paper.

The goal of a scattering calculation can be reduced to that of the calculation of the scattering state $\Psi_{k,\nu}$ of a total Hamiltonian $H=H_{\rm in}+V$, which corresponds to an incoming eigenstate of $H_{\rm in}$, $\Psi^{\rm in}_{k,v}=e^{ikR}\phi_v(r)$. Here, we denote the incoming translational coordinate by R, and the perpendicular coordinates by r. The energy E of the scattering is determined by the incoming quantum numbers: $E_{k,\nu}=E_\nu+\hbar^2k^2/2M_R$. Once $\Psi_{k,\nu}$ is determined, all the relevant physical information concerning the scattering event may be inferred from it: the elastic, inelastic and reactive scattering data is extracted from $\Psi_{k,\nu}$ by considering the relevant asymptotes.

We start by writing $\Psi_{k,q}$ as

$$\Psi_{k,\nu}(r,R)=\chi_{k,\nu}(r,R)+f(R)\Psi^{\rm in}_{k,\nu}. \tag{B1}$$

The function $f(R)$ is chosen such that it equals 1 in the incoming channel, becoming zero in the interaction region where $V(R)\neq 0$ and in the reactive channel. This choice for $f(R)$ ensures that $\chi_{k,\nu}$ will be identical with $\Psi_{k,\nu}-\Psi^{\rm in}_{k,\nu}$ in the asymptotic regions. Thus we refer to $\chi_{k,\nu}$ as ''the scattered wave.'' Using Eq. (B1) the Schrodinger equation now becomes

$$0=(H-E)\Psi_{k,\nu}=(H-E)\chi_{k,\nu}+(H_{\rm in}-E)f\Psi^{\rm in}_{k,\nu}. \tag{B2}$$

Recalling the properties of the function $f(R)$, we obtain the following equation for $\chi_{k,\nu}$:

$$(E-H)\chi_{k,\nu}=-\frac{\hbar^2}{2M_R}\left(\frac{d^2(fe^{ikr})}{dR^2}+k^2f\right)\phi_\nu(r). \tag{B3}$$

In our calculations we chose $f(R)$ as the complementary error function

$$f(R)=1-\frac{1}{\sqrt{2\pi}\sigma}\int_{-\infty}^{R}e^{-(R'-R_0)^2/2\sigma^2}dR', \tag{B4}$$

where R_0 and σ are selected so that $f(R)$ is practically zero in the interaction region. Using the analytical form for $f(R)$ in Eq. (B4), we find the equation for $\chi_{k,\nu}$ of the specific form

$$(E-H)\chi_{k,\nu}=\frac{\hbar^2}{2M_R}\left(\frac{R-R_0}{\sigma^2}+2ik\right)e^{ikR}\frac{e^{-(R-R_0)^2/2\sigma^2}}{\sqrt{2\pi}\sigma}\phi_\nu(r). \tag{B5}$$

Equation (B5) is an inhomogeneous equation, whose source term, denoted $F_{k,\nu}(R,r)$, is a local function, centered at R_0, of width σ.

In order to obtain a stable solution to Eq. (B5), we regularize the equation by adding to the Hamiltonian a negative imaginary potential $-iV_{\rm NIP}$[23,27] localized in the asymptotes. This enables to write the solution to the Eq. (B5) as

$$\chi_{k,\nu}=\mathbf{G}(E)F_{k,\nu}, \tag{B6}$$

where $\mathbf{G}(E)=(E-H')^{-1}=(E-H+iV_{\rm NIP})^{-1}$. The numerical implementation of this operator is performed by expanding it as a series of Chebychev polynomials of the Hamiltonian[24–26]

$$\mathbf{G}(E)=\frac{i}{\hbar}\int_0^\infty e^{i(E-H)t/\hbar}\,dt\approx\sum_{n=0}^{N}b_n(E)T_n(H_{\rm sc}), \tag{B7}$$

where $T_n(\cos\theta)=\cos(n\theta)$ are the Chebychev polynomials, application of which is explained in Ref. 22. The energy dependent coefficients b_n and the scaled Hamiltonian is described in detail in Ref. 24. In principle, $H_{\rm sc}=(H'-C)/L$, where C is the center and L the length of the major axis of an ellipse contained in the lower part of the complex plane, which encloses the complex eigenvalues of H'. The length N of the series in Eq. (B7) depends on the energy range L of the problem. Typically N is proportional to L. In the present calculations N was taken as 4000 for the adiabatic calculations and 15 000 for the diabatic ones.

The scattered wave function $\chi_{k,\nu}(R,r)$ contains the all the outgoing information. The total transmission (reflection) probability can be obtained by integrating the current density $2\hbar M_R^{-1}\,{\rm Im}\,\chi^*(R,r)\partial\chi(R,r)/\partial R$ on r for R in the products (reactants) channel. The state to state transition probability $\nu\rightarrow\nu'$ can also be calculated and is given by

$$P_{\nu\rightarrow\nu'}=\left|\langle\phi_{\nu'}|\chi_{k,\nu}\rangle_{R=\rm const}\right|^2\frac{k_{\nu'}}{k}, \tag{B8}$$

where $k_{\nu'}$ is the wave number of the outgoing asymptotic wave with internal vibration ν'.

[1] R. Englman, *The Jahn–Teller Effect in Molecules and Crystals* (Wiley-Interscience, New York, 1972).
[2] E. Teller, J. Phys. Chem. **41**, 109 (1937).
[3] W. Moffitt and W. Thorson, Phys. Rev. **108**, 1251 (1957).
[4] H. C. Longuet-Higgins, U. Opik, M. H. L. Pryce, and R. A. Sack, Proc. R. Soc. London, Ser. A **244**, 1 (1958).
[5] M. S. Child and H. C. Longuet-Higgins, Philos. Trans. R. Soc. London, Ser. A **254**, 259 (1961).
[6] G. Herzberg and H. C. Longuet-Higgins, Discuss. Faraday Soc. **35**, 77 (1963).
[7] M. Born and J. R. Oppenheimer, Ann. Phys. (Leipzig) **84**, 457 (1927).
[8] (a) W. H. Gerber and E. Schumacher, J. Chem. Phys. **69**, 1692 (1978); (b) W. Duch and G. A. Segal, *ibid.* **79**, 2951 (1983); **82**, 2392 (1985); (c) T. C. Thompson, D. G. Truhlar, and C. A. Mead, *ibid.* **82**, 2392 (1985).
[9] M. Baer and R. Englmann, Mol. Phys. **75**, 293 (1992).
[10] J. Schon and H. Koppel, J. Chem. Phys. **103**, 9292 (1995).
[11] (a) M. Baer, Chem. Phys. Lett. **35**, 112 (1975); (b) Z. H. Top and M. Baer,

J. Chem. Phys. **66**, 1363 (1977); (c) Chem. Phys. **25**, 1 (1977); M. Baer, Mol. Phys. **40**, 1011 (1980).
[12] (a) M. Baer, in *The Theory of Chemical Reaction Dynamics*, edited by M. Baer (CRC, Boca Raton, 1985), Vol. II, Chap. 4; (b) M. Baer, in *State-Selected and State-to-State Ion-Molecule Reaction Dynamics*, edited by M. Baer and C. Y. Ng (Wiley, New York, 1992), Vol. II, Chap. 4; (c) V. Sidis, *ibid.*, Chap. 2; (d) T. Pacher, L. S. Cederbaum, and H. Koppel, Adv. Chem. Phys. **84**, 293 (1993).
[13] (a) H. Koppel, W. Domcke, and L. S. Cederbaum, Adv. Chem. Phys. **57**, 59 (1984); (b) C. A. Mead and D. G. Truhlar, J. Chem. Phys. **77**, 6090 (1982); (c) C. Petrongolo, R. J. Buekener, and S. D. Peyerimhoff, *ibid*. **78**, 7284 (1983); (d) T. J. Gregory, M. L. Steven, D. G. Truhlar, and D. Schwenke, in *Advances in Molecular Vibrations and Collision Dynamics*, edited by J. M. Bowman (JAI, Connecticut, 1994), Vol. 2B, Chap. III; (e) T. Pacher, C. A. Mead, L. S. Cederbaum, and H. Koppel, J. Chem. Phys. **91**, 7057 (1989).
[14] (a) C. A. Mead, J. Chem. Phys. **72**, 3839 (1980); (b) D. G. Truhlar and C. A. Mead, *ibid*. **70**, 2284 (1979).
[15] (a) Y.-S. M. Wu, A. Kuppermann, and B. Lepetit, Chem. Phys. Lett. **186**, 319 (1991); (b) A. Kuppermann and Y.-S. M. Wu, *ibid*. **205**, 577 (1993); (c) Y.-S. M. Wu and A. Kuppermann, *ibid*. **235**, 105 (1995); (d) X. Wu, R. E. Wyatt, and M. D'mello, J. Chem. Phys. **101**, 2953 (1994); (e) N. Markovic and G. D. Billing, *ibid*. **101**, 2953 (1994).
[16] Y. Aharonov and D. Bohm, Phys. Rev. **115**, 485 (1959).
[17] M. V. Berry, Proc. Soc. London, Ser. A **392**, 45 (1984).
[18] M. Baer and R. Englman (unpublished).
[19] C. Eckart, Phys. Rev. **35**, 1303 (1930).
[20] M. Gilibert and M. Baer, J. Phys. Chem. **99**, 15748 (1995).
[21] (a) M. Gilibert, A. Baram, H. Szichman, and M. Baer, J. Chem. Phys. **99**, 3503 (1993); (b) E. Eisenberg, S. Ron, and M. Baer, *ibid*. **101**, 3802 (1994); (c) E. Eisenberg, D. M. Charutz, S. Ron, and M. Baer, *ibid*. **104**, 1886 (1996).
[22] R. Kosloff, J. Phys. Chem. **92**, 2087 (1988).
[23] R. Kosloff and D. Kosloff, J. Comput. Phys. **63**, 363 (1986).
[24] Y. Huang, D. J. Kouri, and D. K. Hoffman, J. Chem. Phys. **101**, 10493 (1994).
[25] O. Citri, R. Baer, and R. Kosloff, Surf. Sci. (in press).
[26] R. Baer, Y. Zeiri, and R. Kosloff (unpublished).
[27] D. Neuhauser and M. Baer, J. Chem. Phys. **90**, 4351 (1989).